Electronic Supplementary Information

Anion-coordination-driven single-double helix switching and chiroptical molecular switch based on oligoureas

Hongfei Li,‡[a] Lei Kou,‡[a] Lin Liang,[b] Boyang Li,[a] Wei Zhao,*[b] Xiao-Juan Yang[b] and Biao Wu*[ab]

[a] Key Laboratory of Synthetic and Natural Functional Molecule Chemistry of the Ministry of Education, College of Chemistry and Materials Science, Northwest University, Xi'an 710069, China.

[b] Key Laboratory of Medical Molecule Science and Pharmaceutics Engineering, Ministry of Industry and Information Technology, School of Chemistry and Chemical Engineering, Beijing Institute of Technology, Beijing 102488, China

Table of contents:

S1. General Methods

All the reagents were obtained from commercial suppliers and used as received unless otherwise indicated. The solvents and other reagents were of reagent grade and purchased commercially. ^{1}H NMR spectra were obtained by using Bruker AVANCE III-400 MHz spectrometers under 298 K. ^{1}H NMR chemical shifts were reported relative to residual solvent peaks (2.50 *ppm* for DMSO-*d6*). The mass spectra of ligands and complexes were measured with a Bruker microTOF-Q II ESI-Q-TOF LC/MS/MS spectrometer. Circular Dichroism (CD) spectra and corresponding ultraviolet absorption spectra were recorded on a J-1500 spectropolarimeter (Jasco, Japan) at 298 K, using a 3 cm quartz cuvette. X-ray diffractions were recorded on a Bruker D8 Venture Photon II diffractometer and BL17B macromolecular crystallography beamline.

S2. Synthetic Procedures of Oligourea Ligands

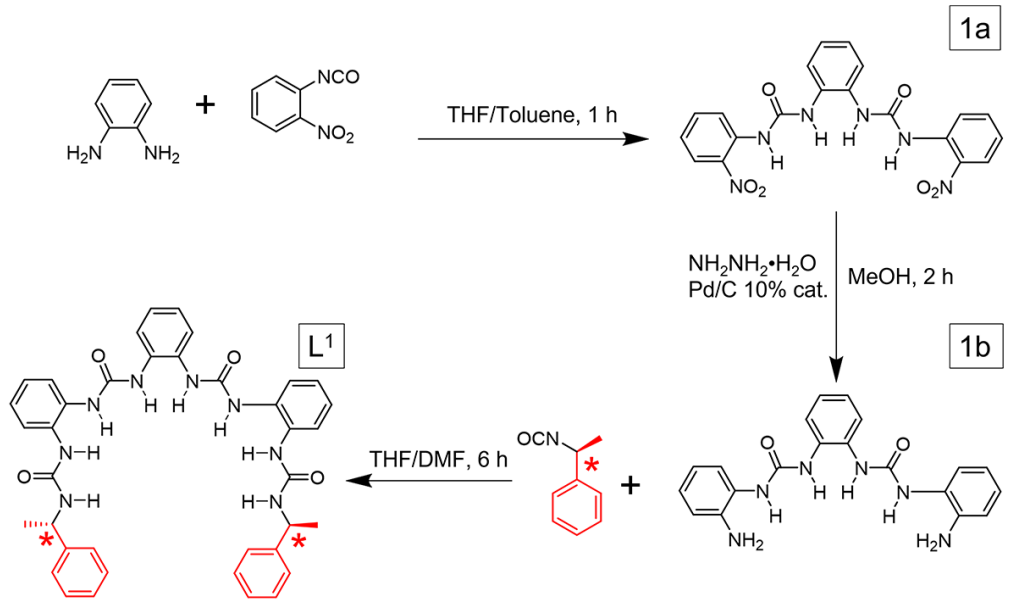

Scheme S1. Synthetic scheme of preparing tetra-urea chiral ligand **L^1**.

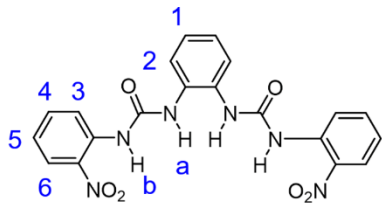

1a: 1,2-Bis-(2-nitrophenyl-urea)-benzene. 1,2-diaminobenzene (1.0 g, 9.2 mmol) dissolved in tetrahydrofuran (THF, 200 mL) was added to a solution of *o*-nitro-phenylisocyanate (3.3 g, 20.0 mmol) in 80 mL THF. The precipitate thus formed was filtered off and washed several times with toluene and diethyl ether, and then dried over vacuum to get

pure **1a** as a yellow solid, yield: 90 %. ^{1}H NMR (400 MHz, DMSO-*d6*, ppm): δ 9.75 (s, 1H, Hb), 9.18 (s, 1H, Ha), 8.25 (d, J = 8.4 Hz,1H, H3), 8.06 (d, J = 8.4 Hz, 1H, H6), 7.70 (dd, J = 8.0 Hz, H4), 7.60 (dd, J = 8.0 Hz, 1H, H5), 7.21 (d, J = 7.6 Hz, 1H, H2), 7.14 (dd, J = 7.6 Hz, 1H, H1).

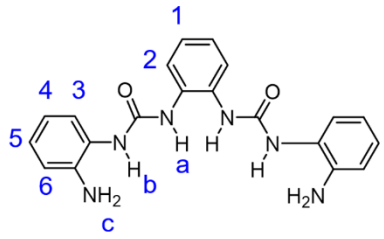

1b: 1,2-Bis-(2-aminophenyl-urea)-benzene. Hydrazine monohydrate (5.0 mL) was added dropwise to the suspension of **1a** (2.2 g, 5.1 mmol) and Pd/C (0.20 g, 10% cat.) in ethanol (200 mL) under stirring overnight. Whereafter, the solid was filtered off *via* suction filtration and then dissolved in a small amount of dimethylformamide (DMF) and filtered through Celite to remove Pd/C. Diethyl ether (200 mL) was poured into the DMF solution after which the obtained precipitate was filtered off, washed several times with ethanol and diethyl ether and dried over vacuum, and finally to give **1b** as a white solid (1.3 g, 3.5 mmol, 69 %). ^{1}H NMR (400 MHz, DMSO-*d6*, ppm): δ 8.14 (s, 1H, Ha), 8.10 (s, 1H, Hb), 7.57 (dd, J = 6.0 Hz, 1H, H1), 7.32 (d, J = 8.0 Hz, 1H, H2), 7.06 (dd, J = 5.2 Hz, 1H, H5), 6.85 (dd, J = 7.2 Hz, 1H, H4), 6.75 (d, J = 8.0 Hz, 1H, H3), 6.57 (d, J = 8.0 Hz, 1H, H6), 4.81 (s, 2H, Hc).

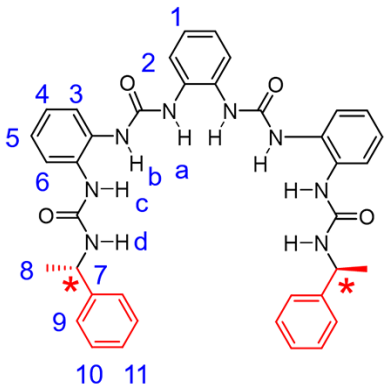

Tetra-urea **L^{1}**: (S)-(-)-α-methylbenzyl isocyanate (367 mg, 2.5 mmol) was added to a DMF (5 mL) solution of compound **1b** (376 mg, 1 mmol). After stringing overnight, the resulting precipitate was filtered off and washed several times with ethanol and diethyl ether. Then, the product was dried under vacuum to yield **L^{4S}** as a white solid. (584 mg), yield: 87%. ^{1}H NMR (400 MHz, DMSO-*d6*, ppm): δ 8.39 (s, 2H, Hc, Hb), 7.87 (s, 1H, Ha), 7.62 (m, J = 8.0 Hz, 2H, H3, H6), 7.43 (d, J = 8.0 Hz, 1H, H2), 7.32 (m, 4H, H9, H10), 7.22 (m, 1H, H11), 7.10 (m, 4H, Hd, H1, H4, H5), 4.80 (m, 1H, H7), 1.36 (d, J = 7.2 Hz, 3H, H8). ^{13}C NMR (400 MHz, DMSO-d6, ppm): δ 154.93 (CO), 154.21 (CO), 145.16 (C), 133.07 (C), 131.40 (C), 129.47 (C), 128.34 (CH), 126.69 (CH), 125.94 (CH), 125.03 (CH), 124.43 (CH), 124.14 (CH), 123.97 (CH), 122.65 (CH), 122.30 (CH), 48.33 (CH), 23.13 (CH_3). ESI-MS: m/z, 100%, 693.2959 $[M+Na]^+$; 42%, 709.2638 $[M+K]^+$.

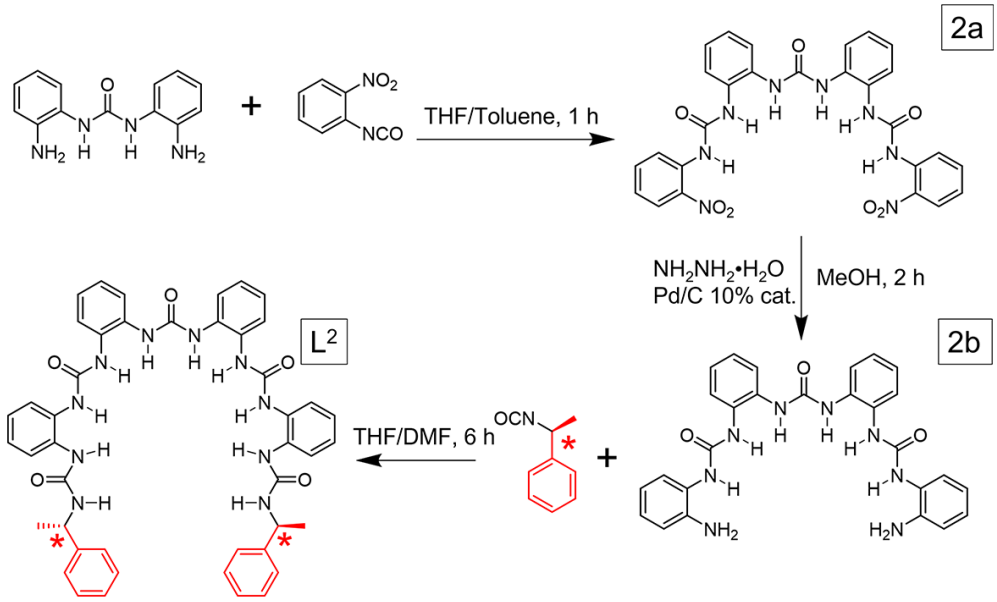

Scheme S2. Synthetic scheme of preparing pentakis-urea chiral ligand **L²**.

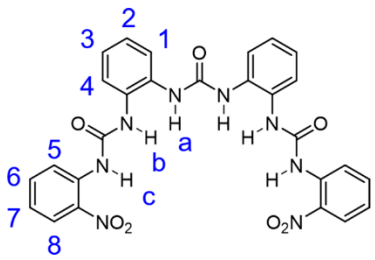

2a: To a solution of 1,3-Bis(2-aminophenyl)urea (1.2 g, 5.0 mmol) in DMF (15 mL) in N_2 atmosphere, a solution of *o*-nitro-phenylisocyanate (1.8 g, 11.5 mmol) in THF (7 mL) was added dropwise at 70 ℃. After stirring at the same temperature for 1 h, the solvents were evaporated by reduced pressure and washed for several times with ethanol and diethyl ether. A yellow solid (2.6 g) was produced as the **2a**, yield: 92%. ^{1}H NMR (400 MHz, DMSO-*d6*, ppm): δ 9.75 (s, 1H, NHc), 9.21 (s, 1H, NHb), 9.51 (s, 1H, NHa), 8.24 (d, J = 8.4 Hz, 1H, H8), 8.05 (d, J = 8.0 Hz, 1H, H5), 7.73 (d, J = 8.0 Hz, 1H, H4), 7.65 (dd, J = 8.0 Hz, 1H, H6), 7.48 (d, J = 7.6 Hz, 1H, H1), 7.16 (m, 2H, H3, H7), 7.07 (dd, J =7.6 Hz, 1H, H2).

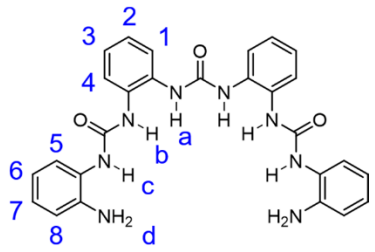

2b: Hydrazine monohydrate (5.0 mL) was added dropwise to the suspension of **2a** (2.2 g, 4.3 mmol) and Pd/C (0.20 g, 10% cat.) in ethanol (200 mL) under stirring 2 h. Whereafter, the solid was filtered off *via* suction filtration and then dissolved in DMF (20 ml) and filtered through Celite to remove Pd/C. Diethyl ether (200 mL) was poured into the DMF solution after which the obtained precipitate was filtered off, washed several times with ethanol and diethyl ether and dried over vacuum. Finally, a white solid (1.5 g) was produced as the **2b**, yield: 65%. ^{1}H NMR (400 MHz, DMSO-*d6*, ppm): 8.45 (s, 1H, NHa),

8.16 (s, 1H, NHb), 8.15 (s, 1H, NHc), 7.60 (d, J = 6.4 Hz, 1H, H1), 7.55 (d, J = 2.4 Hz, 1H, H4), 7.30 (d, J = 5.2 Hz, 1H, H5), 7.06 (m, 2H, H2, H3), 6.84 (dd, J = 7.6 Hz, 1H, H7), 6.73 (d, J = 5.6 Hz, 1H, H8), 6.55 (dd, J = 4.8 Hz, 1H, H6), 4.82 (s, 2H, NHd).

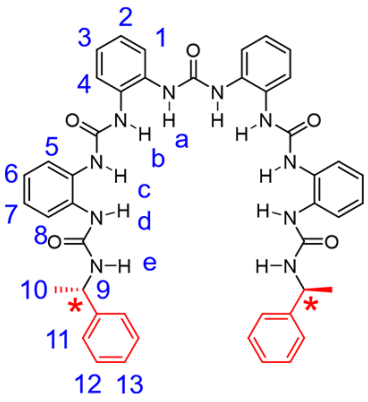

Pentakis-urea **L²**: (S)-(-)-α-methylbenzyl isocyanate (367 mg, 2.5 mmol) was added to a DMF (5 mL) solution of compound **1b** (510 mg, 1 mmol). After stringing overnight, the resulting precipitate was filtered off and washed several times with ethanol and diethyl ether. Then, the product was dried under vacuum to yield **L^5S** as a white solid (611 mg), yield: 76%. ^{1}H NMR (400 MHz, DMSO-*d6*, ppm): δ 8.49 (s, 1H, Hb), 8.42 (br, 2H, Hc, Hd), 7.86 (s, 1H, Ha), 7.61 (m, 3H, H1, H4, H5), 7.40 (d, J = 8.0 Hz, 1H, H8), 7.32 (m, 4H, H11, H12), 7.06 (m, 6H, He, H2, H3, H6, H7, H13), 4.80 (m, 1H, H9), 1.35 (d, J = 7.6 Hz, 3H, H10). ^{13}C NMR (400 MHz, DMSO-*d6*, ppm): δ 154.93 (CO), 154.18 (CO), 154.11 (CO), 145.15 (C), 133.02 (C), 131.57 (C), 131.10 (C), 129.50 (C), 128.33 (CH), 126.68 (CH), 125.93 (CH), 124.95 (CH), 124.41 (CH), 124.35 (CH), 124.07 (CH), 123.98 (CH), 123.87 (CH), 122.68 (CH), 122.36 (CH), 48.82 (CH), 23.13 (CH_3). ESI-MS: m/z, 100%, 827.3440 $[M+Na]^+$; 39%, 805.3580 $[M+H]^+$.

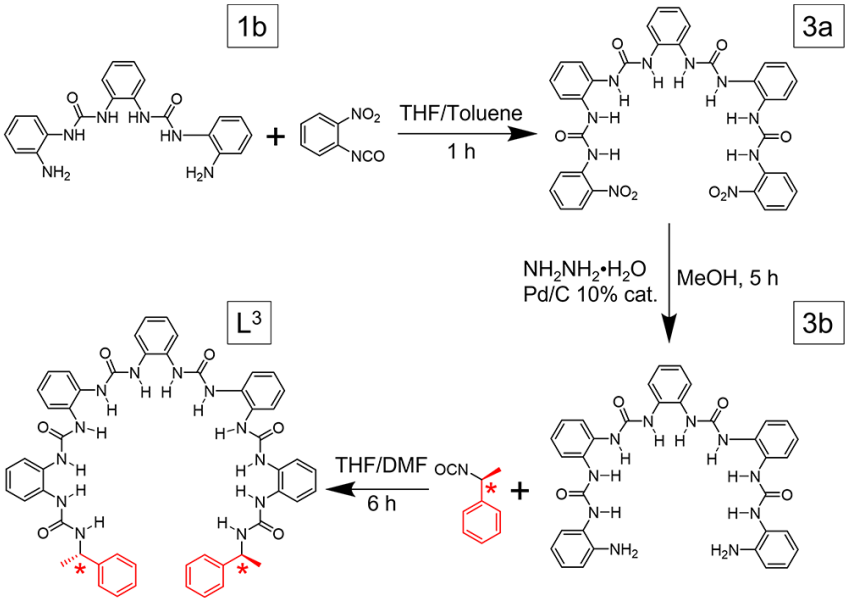

Scheme S3. Synthetic scheme of preparing hexa-urea chiral ligand **L³**.

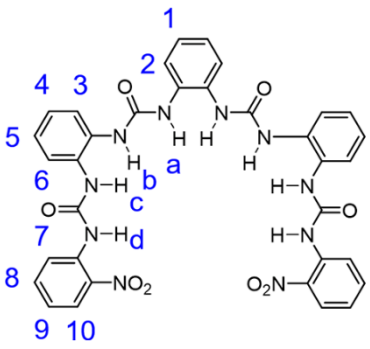

3a: To a solution of **1b** (1.9 g, 5.0 mmol) in DMF (25 mL) in N_2 atmosphere, a solution of *o*-nitro-phenylisocyanate (1.8 g, 11.5 mmol) in THF (7 mL) was added dropwise at 70 ℃. After stirring at the same temperature for 1 h, the solvents were evaporated by reduced pressure and washed for several times with ethanol and diethyl ether. A yellow solid (3.2 g) was produced as the **3a**, yield: 90%. ^{1}H NMR (400 MHz, DMSO-*d6*, ppm): δ 9.74 (s, 1H, NHd), 9.21 (s, 1H, NHc), 8.54 (s, 1H, NHb), 8.47 (s, 1H, NHa), 8.25 (d, J = 8.0 Hz, 1H, H10), 8.07 (d, J = 7.6 Hz, 1H, H7), 7.73 (d, J = 8.0 Hz, 1H, H6), 7.65 (t, J = 8.0 Hz, 1H, H8), 7.57 (d, J = 8.0 Hz, 1H, H3), 7.43 (d, J = 6.8 Hz, 1H, H2), 7.19 (dd, 1H, J = 8.0 Hz, 1H, H9), 7.11, (dd, J = 8.0 Hz, 1H, H4), 7.04 (m, 2H, H1, H5).

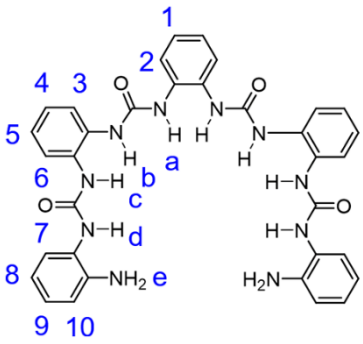

3b: Hydrazine monohydrate (5.0 mL) was added dropwise to the suspension of **1b** (2.2 g, 3.1 mmol) and Pd/C (0.20 g, 10% cat.) in ethanol (200 mL) under stirring 2 h. Whereafter, the solid was filtered off *via* suction filtration and then dissolved in DMF (20 ml) and filtered through Celite to remove Pd/C. Diethyl ether (200 mL) was poured into the DMF solution after which the obtained precipitate was filtered off, washed several times with ethanol and diethyl ether and dried over vacuum. Finally, a white solid (1.3 g) was produced as the **2b**, yield: 65 %. ^{1}H NMR (400 MHz, DMSO-*d6*, ppm): δ 8.48 (s, 1H, NHa), 8.46 (s, 1H, NHb), 8.15 (s, 1H, NHc), 8.14 (s, 1H, NHd), 7.59 (m, 2H, H2, H3), 7.52 (d, J = 7.2 Hz, 1H, H6), 7.29 (d, J = 7.2 Hz, 1H, H7), 7.04 (m, 3H, H1, H4, H9), 6.83 (t, J = 6.8 Hz, 1H, H5), 6.72 (d, J = 7.2 Hz, 1H, H10), 6.54 (t, J = 7.2 Hz, 1H, H8), 4.78 (s, 2H, NHe).

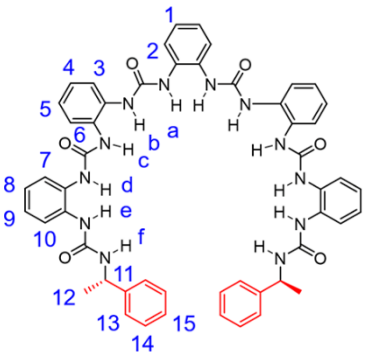

Hexa-urea **L^3**: (S)-(-)-α-methylbenzyl isocyanate (367 mg, 2.5 mmol) was added to a DMF (5 mL) solution of compound **3b** (645 mg, 1 mmol). After stringing overnight, the resulting precipitate was filtered off and washed several times with ethanol and diethyl ether. Then, the product was dried under vacuum to yield **L^{6S}** as a white solid (572 mg), yield: 61%. ^{1}H NMR (400 MHz, DMSO-*d6*, ppm): δ 8.52 (s, 2H, He), 8.50 (s, 2H, Hd), 8.41 (s, 2H, Hc, Hb),

7.86 (s, 1H, Ha), 7.63 (m, 4H, H2, H3, H6, H7), 7.41 (d, J = 8.0 Hz, 1H, H10), 7.31 (m, 4H, H13, H14), 7.21 (m, 1H, H15), 7.12 (m, 6H, Hf, H1, H4, H5, H8, H9), 4.80 (m, 1H, H11), 1.36 (d, J = 6.8 Hz, 3H, H12). ^{13}C NMR (400 MHz, DMSO-*d6*, ppm): δ 154.93 (CO), 154.19 (CO), 154.10 (CO), 145.16 (C), 133.08 (C), 131.58 (C), 131.28 (C), 131.08 (C), 129.47 (C), 128.34 (CH), 126.69 (CH), 125.93 (CH), 125.01 (CH), 124.18 (CH), 124.07 (CH), 124.00 (CH), 123.88 (CH), 122.67 (CH), 122.34 (CH), 48.83 (CH), 21.13 (CH_3). ESI-MS: m/z, 100%, 961.3899 $[M+Na]^+$; 30%, 977.3658 $[M+K]^+$.

S3. Preparations of Anion Coordination Driven Complexes

Crystal $(TEA)_2[\mathbf{L^1}\bullet Cl_2]$: (TEA)Cl solution (32 μL, 0.625 mol/L, in acetonitrile) was added to a suspension of $\mathbf{L^1}$ (6.70 mg, 10 mmol) in chloroform. After stirring overnight at room temperature, a colorless solution was obtained. Slow vapor diffusion of diethyl ether into this solution provided colorless crystals of $(TEA)_2[\mathbf{L^1}\bullet Cl_2]$ within two weeks. The crystal was directly mounted on a diffractometer for data collections.

Crystal $(TBA)_2[\mathbf{L^2}\bullet Cl_2]$: (TBA)Cl solution (20 μL, 0.625 mol/L, in acetonitrile) was added to a suspension of $\mathbf{L^2}$ (5 mg, 6.2 mmol) in chloroform. After stirring overnight at room temperature, a clearly colorless solution was obtained. Slow vapor diffusion of diethyl ether into this solution provided yellow crystals of $(TBA)_2[\mathbf{L^2}\bullet Cl_2]$ within two weeks. The crystal was directly mounted on a diffractometer for data collections.

Crystal $(TMA)_3[\mathbf{L^1}_2\bullet PO_4]$: $(TMA)_3PO_4$ solution (8 μL, 0.625 mol/L, in water) was added to a suspension of $\mathbf{L^1}$ (6.7 mg, 10 mmol) in mixed solution of acetone and acetonitrile. After stirring overnight at room temperature, a colorless solution was obtained. Slow vapor diffusion of diethyl ether into this solution provided colorless crystals of $(TMA)_3[\mathbf{L^1}_2\bullet PO_4]$ within one week. The crystal was directly mounted on a diffractometer for data collections.

Crystal $(TMA)_3[\mathbf{L^3}\bullet PO_4\bullet(H_2O)_2]$: $(TMA)_3PO_4$ solution (8.6 μL, 0.625 mol/L, in water) was added to a suspension of $\mathbf{L^3}$ (5 mg, 5.3 mmol) in acetone. After stirring overnight at room temperature, a colorless solution was obtained. Slow vapor diffusion of diethyl ether into this solution provided colorless crystals of $(TMA)_3[\mathbf{L^3}\bullet PO_4\bullet(H_2O)_2]$ within two weeks.

According to general method of crystal growth, we respectively attempted to synthesize crystals of supermolecule complex $[\mathbf{L^3}\bullet Cl_2]^{2-}$, $[\mathbf{L^2}_2\bullet PO_4]^{3-}$ and $[\mathbf{L^2}\bullet PO_4]^{3-}$ using the slow vapor diffusion of poor solvent. Unfortunately, crystals with better diffraction points have never been

obtained. However, we still used other detection methods (^{1}H NMR, ESI-MS and CD spectrum) to prove the assembly configuration and structure information of complexes $[\mathbf{L^3}\bullet Cl_2]^{2-}$, $[\mathbf{L^2}_2\bullet PO_4]^{3-}$ and $[\mathbf{L^2}\bullet PO_4]^{3-}$.

S4. X-ray Diffraction Data

X-ray diffraction data of crystals $(TBA)_2[\mathbf{L^2}\bullet Cl_2]$, $(TMA)_3[\mathbf{L^1}_2\bullet PO_4]$ and $(TMA)_3[\mathbf{L^3}\bullet PO_4\bullet(H_2O)_2]$ were detected on a Bruker D8 Venture Photon II diffractometer with graphite-monochromatic Mo Kα radiation (λ = 0.71073 Å) under 150 K. The diffraction data for crystal $(TEA)_2[\mathbf{L^1}\bullet Cl_2]$ were collected at the BL17B macromolecular crystallography beamline in Shanghai Synchrotron Facility (λ = 0.72929 Å). An empirical absorption correction using SADABS was applied for all data. (SADABS v 2018. 1, Bruker AXS, Madison, WI, **2018**.) The structures were solved by the dual methods *via* SHELXS program. (A short history of SHELX, G. M. Sheldrick, *Acta Cryst.*. **2008**, A*64*, 112-122). All structures were solved and refined to convergence by the full-matrix least-squares on F^2 for all independent reflections by the use of the program SHELXL. Hydrogen atoms were included in idealized positions with thermal parameters equivalent to 1.2 times those of the atom to which they were attached. Thereinto, because the structure of crystal $(TEA)_2[\mathbf{L^1}\bullet Cl_2]$ is small and the light source of BL17B macromolecular crystallography beamline is too strong, the low-angle diffraction points were overexposure, which leads to the low completeness of the crystal structure. All the crystal structures have been deposited with the Cambridge Crystallographic Data Centre (CCDC), and their corresponding CCDC number are shown in Table S1 and S2.

Table S1. Crystal data and refinement details of complexes **1** and **2**

Complexes	$(TEA)_2[\mathbf{L^1}\bullet Cl_2]$	$(TBA)_2[\mathbf{L^2}\bullet Cl_2]$
CCDC Number	2130743	2130744
Formula	$C_{54}H_{78}Cl_2N_{10}O_4$	$C_{77}H_{44}Cl_2N_{12}O_5$
M	1002.16	1288.14
Crystal system	Monoclinic	Monoclinic
Space group	$C2$	$P2_1$
a (Å)	20.7990(5)	11.9428(5)
b (Å)	14.2717(4)	25.5121(9)
c (Å)	20.0159(6)	12.5127(4)
α (deg)	90	90
β (deg)	114.881(1)	92.975(1)
γ (deg)	90	90
V (Å^3)	5390.0(3)	3807.3(2)
Z	4	2
T (K)	150	150
F(000)	2152	1328
D_{calc} (g·cm^{-3})	1.235	1.124
R(int)	0.0508	0.0596
Data/restraints/parameters	8941 / 1 / 641	13393 / 1 / 875
GOF	1.062	0.732
$R1$ [$I > 2\sigma(I)$]	0.0393	0.0425
$wR2$ [$I > \sigma(I)$]	0.1036	0.1156

Table S2. Crystal data and refinement details of complexes **4** and **6**

Complexes	$(TMA)_3[\mathbf{L^1}_2 \bullet PO_4]$	$(TMA)_3[\mathbf{L^3} \bullet PO_4 \bullet (H_2O)_2]$
CCDC Number	2130745	2130746
Formula	$C_{198}H_{239}N_{40}O_{31}P_2$	$C_{67}H_{96}N_{15}O_{13}P$
M	3737.22	3625.26
Crystal system	Triclinic	Monoclinic
Space group	$P1$	$P2_1$
a (Å)	13.8456(13)	13.0070(12)
b (Å)	13.8504(12)	20.8259(16)
c (Å)	26.594(2)	13.9625(14)
α (deg)	98.630(3)°	90°
β (deg)	90.112(3)°	106.566(3)°
γ (deg)	101.910(3)°	90°
V (Å^3)	4930.7(8)	3625.2(6)
Z	1	2
T (K)	149.98	150
F(000)	1985	1444
D_{calc} (g·cm^{-3})	1.266	1.237
R(int)	0.1269	0.0670
Data/restraints/parameters	35990 / 306 / 2472	12829 / 1 / 867
GOF	1.001	1.038
$R1$ [$I > 2\sigma(I)$]	0.0726	0.0954
$wR2$ [$I > \sigma(I)$]	0.1712	0.2187

Table S3. Hydrogen bond parameters [Å and °] in the crystal structure of $(TEA)_2[\mathbf{L^1}\bullet Cl_2]$.

D-H· · · A	d(D-H)	d(H· · · A)	d(D· · · A)	∠(DHA)
N1-H1· · · Cl1	0.86	2.32	3.170(4)	167
N2-H2· · · Cl1	0.86	2.43	3.211(2)	151
N3-H3· · · Cl1	0.86	2.41	3.235(3)	161
N4-H4· · · Cl1	0.86	2.65	3.431(6)	150
N5-H5· · · Cl2	0.86	2.65	3.431(5)	150
N6-H6· · · Cl2	0.86	2.42	3.281(4)	161
N7-H7· · · Cl2	0.86	2.43	3.213(2)	151
N8-H8· · · Cl2	0.86	2.32	3.172(7)	167

Table S4. Hydrogen bond parameters [Å and °] in the crystal structure of $(TBA)_2[\mathbf{L^2}\bullet Cl_2]$.

D-H· · · A	d(D-H)	d(H· · · A)	d(D· · · A)	∠(DHA)
N1-H1· · · Cl1	0.86	2.43	3.252(3)	161
N2-H2· · · Cl1	0.86	2.36	2.752(3)	108
N3-H3· · · Cl2	0.86	2.51	3.318(3)	157
N4-H4· · · Cl2	0.86	2.44	3.265(2)	162
N5-H5· · · Cl1	0.86	2.49	3.319(3)	163
N6-H6· · · Cl1	0.86	2.55	3.333(3)	153
N7-H7· · · Cl2	0.86	2.69	3.475(3)	153
N8-H8· · · Cl1	0.86	2.7	3.423(2)	143
N9-H9· · · Cl2	0.86	2.73	3.537(3)	158
N10-H10· · · Cl2	0.86	2.51	3.332(3)	160

Table S5. Hydrogen bond parameters [Å and °] in the crystal structure of $(TMA)_3[\mathbf{L^1}_2\bullet PO_4]$.

D-H· · · A	d(D-H)	d(H· · · A)	d(D· · · A)	∠(DHA)
N1-H1A· · · O20	0.88	2.02	2.853(7)	157
N2-H2A· · · O20	0.88	2.24	3.021(7)	148
N3-H3A· · · O17	0.88	2.11	2.865(7)	144
N4-H4A· · · O17	0.88	2.09	2.708(7)	127
N5-H5A· · · O17	0.88	2.00	2.845(7)	162
N6-H6· · · O19	0.88	1.94	2.784(7)	160
N7-H7A· · · O19	0.88	1.96	2.833(7)	169
N8-H8· · · O18	0.88	2.10	2.899(7)	151
N9-H9· · · O18	0.88	2.30	3.023(7)	140
N10-H10· · · O18	0.88	1.90	2.726(7)	157
N11-H11A· · · O18	0.88	2.20	2.986(7)	149
N12-H12A· · · O20	0.88	1.84	2.717(7)	171
N13-H13A· · · O20	0.88	2.17	2.853(7)	135
N14-H14A· · · O19	0.88	1.85	2.717(7)	169
N15-H15· · · O19	0.88	2.10	2.951(7)	162
N16-H16· · · O17	0.88	2.02	2.884(7)	168

Table S6. Hydrogen bond parameters [Å and °] in the crystal structure of $(TMA)_3[\mathbf{L^3}\bullet PO_4\bullet(H_2O)_2]$.

D-H· · · A	d(D-H)	d(H· · · A)	d(D· · · A)	∠(DHA)
N1-H1· · · O10	0.88	2.1	2.920(4)	154
N2-H2· · · O7	0.88	1.82	2.694(2)	171
N3-H3· · · O7	0.88	2.04	2.872(1)	157
N4-H4· · · O8	0.88	1.98	2.793(1)	153
N5-H5· · · O8	0.88	1.89	2.755(0)	167
N6-H6· · · O10	0.88	2.05	2.892(2)	159
N7-H7· · · O10	0.88	1.8	2.666(2)	166
N8-H8· · · O9	0.88	2.26	3.111(2)	162
N9-H9· · · O9	0.88	1.78	2.656(2)	174
N10-H10· · · O11	0.88	2.35	2.753(4)	153
N11-H11· · · O7	0.88	1.96	2.781(1)	155
N12-H12· · · O7	0.88	2.07	2.836(1)	144

Table S7. Hydrogen bonds (Å and deg) involved in chloride binding and Cl· · · Cl separations in the crystal structures of complexes $(TEA)_2[\mathbf{L^1}\bullet Cl_2]$ and $(TBA)_2[\mathbf{L^2}\bullet Cl_2]$.

	Cl1		Cl2		
Complex	H-bond number	Average *d*(N· · · Cl) and ∠(NHCl) (Å, deg)	H-bond number	Average *d*(N· · · Cl) and∠ (NHCl) (Å, deg)	Cl1· · · Cl2 separation[A˚]
$(TEA)_2[\mathbf{L^1}\bullet Cl_2]$	4	3.26, 157	4	3.28, 157	4.21
$(TBA)_2[\mathbf{L^2}\bullet Cl_2]$	5	3.22, 145	5	3.39, 158	3.73

Table S8. Hydrogen bonds (Å and deg) involved in phosphate binding in the crystal structures of complexes $(TMA)_3[\mathbf{L^1}_2\bullet PO_4]$ and $(TMA)_3[\mathbf{L^3}\bullet PO_4\bullet(H_2O)_2]$.

Complex	H-bond number	average *d*(N· · · O) and ∠(NHO)
$(TMA)_3[\mathbf{L^1}_2\bullet PO_4]$	16	2.85, 154
$(TMA)_3[\mathbf{L^3}\bullet PO_4\bullet(H_2O)_2]$	12	2.81, 160

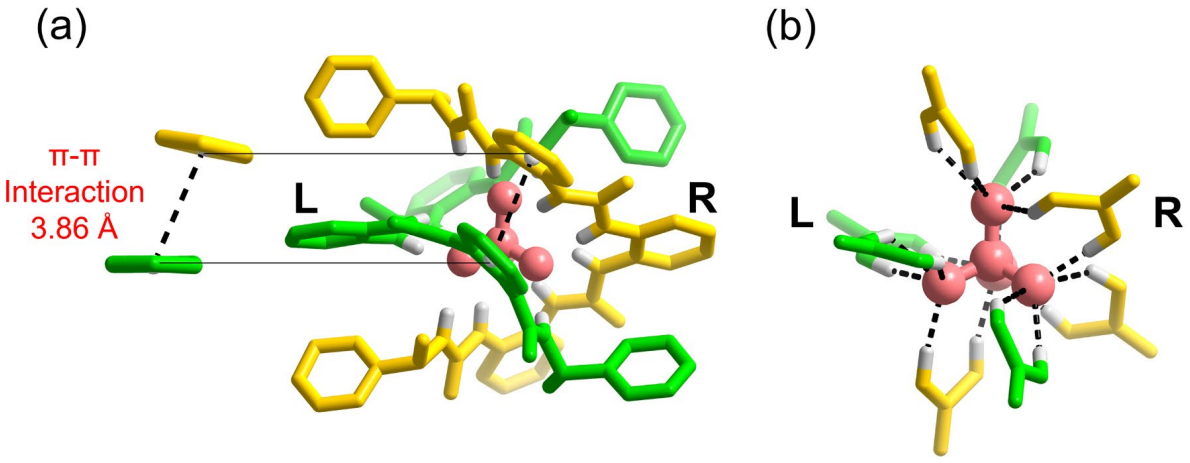

Figure S1. (a) Double helix structure of phosphate-template $[\mathbf{L^1}_2 \bullet PO_4]^{3-}$ complex and (b) corresponding urea groups and hydrogen bond distribution around phosphate (the left and right ligands of double helix are shown in green and yellow, respectively). Selected intermolecular short-contacts (π-π interaction) is shown.

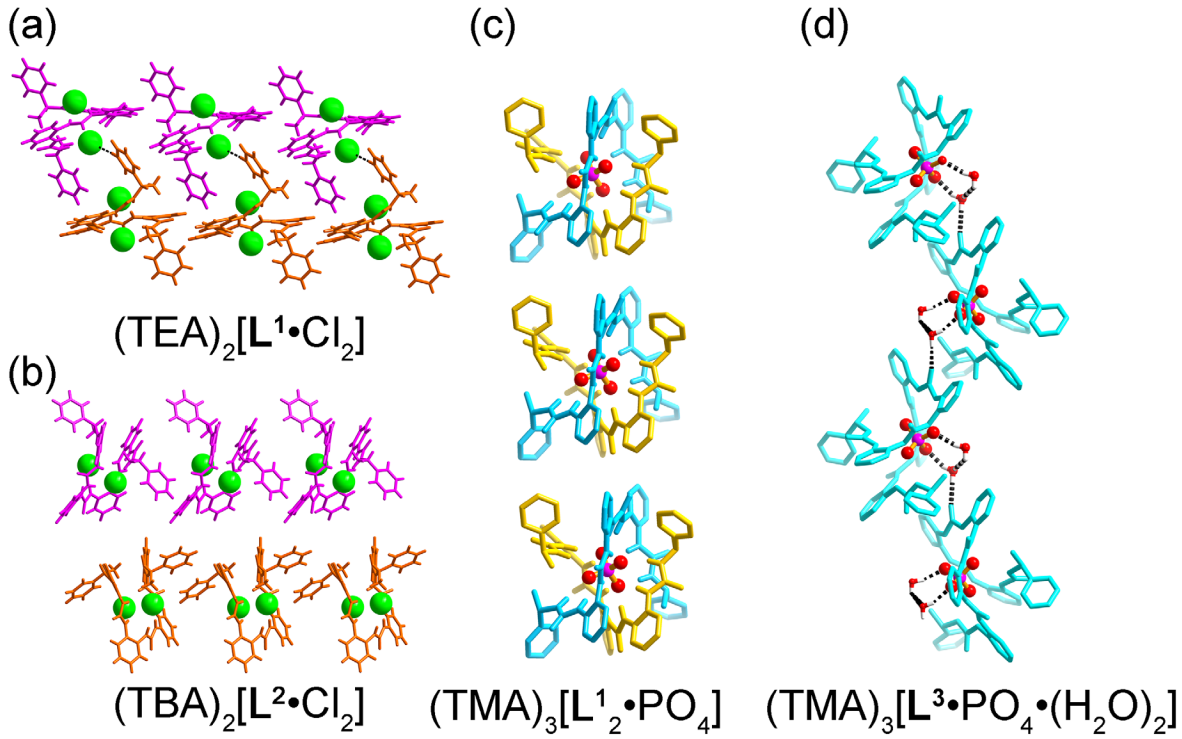

Figure S2. Packing structures of crystals (a) $(TEA)_2[\mathbf{L^1} \bullet Cl_2]$, (b) $(TBA)_2[\mathbf{L^2} \bullet Cl_2]$, (c) $(TMA)_3[\mathbf{L^1}_2 \bullet PO_4]$ and (d) $(TMA)_3[\mathbf{L^3} \bullet PO_4 \bullet (H_2O)_2]$ (chloride ions are shown as green sphere).

S5. Studies of CD and UV-vis Experiments

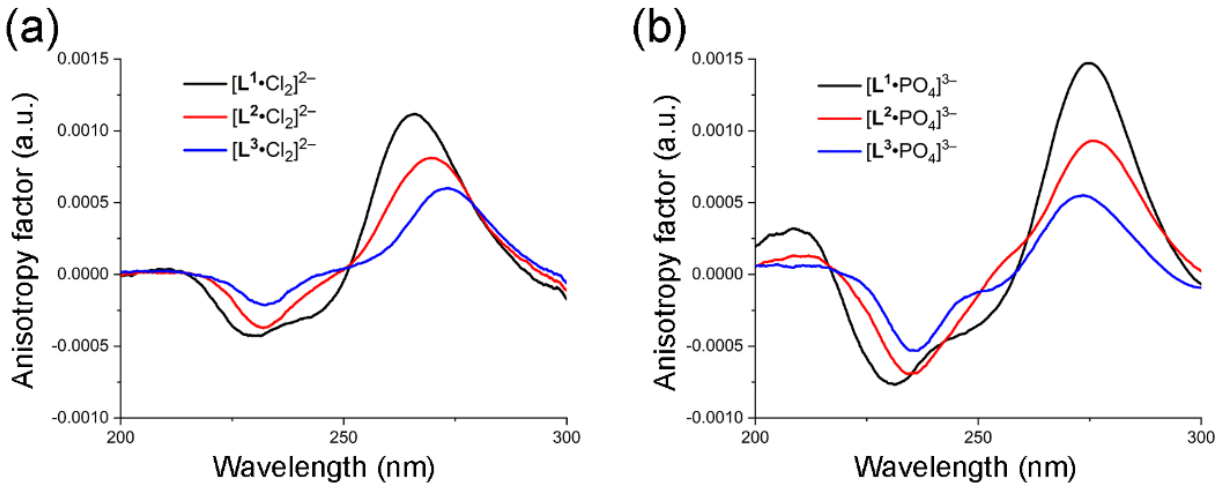

Figure S3. The corresponding anisotropy factors for the single helix of (a) $[L{\bullet}Cl_2]^{2-}$ and (b) $[L{\bullet}PO_4]^{3-}$complexes in acetonitrile ([**L**] = 30 μM). The anisotropy factor $g = \Delta A/A = \theta$[mdeg]/(32980×A). (I. Dolamic, S. Knoppe, A. Dass and T. Bürgi, *Nat. Commun.*, **2012**, 3, 798.)

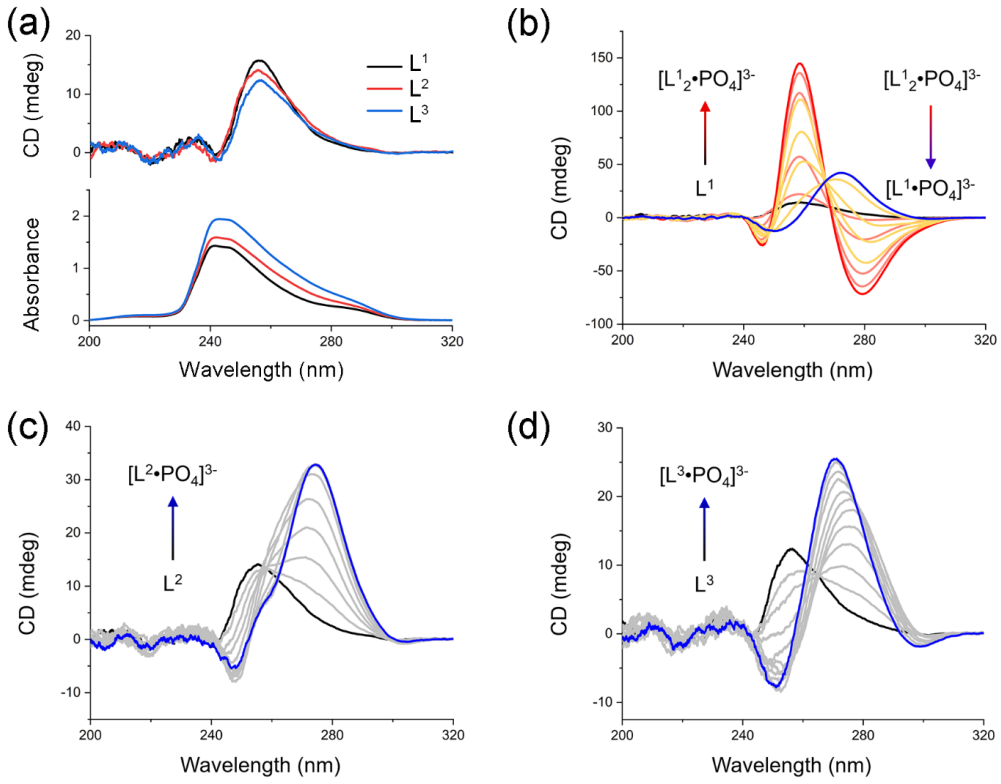

Figure S4. CD spectra of (a) **L¹**, **L²** and **L³** ligands. CD titration of (b) **L¹**, (c) **L²** and (d) **L³** ([**L**] = 30 μM, in 5% v/v DMSO/CH_3CN) by adding 1.2 equivalent of phosphate anions gradually showing conversion in helical sense.

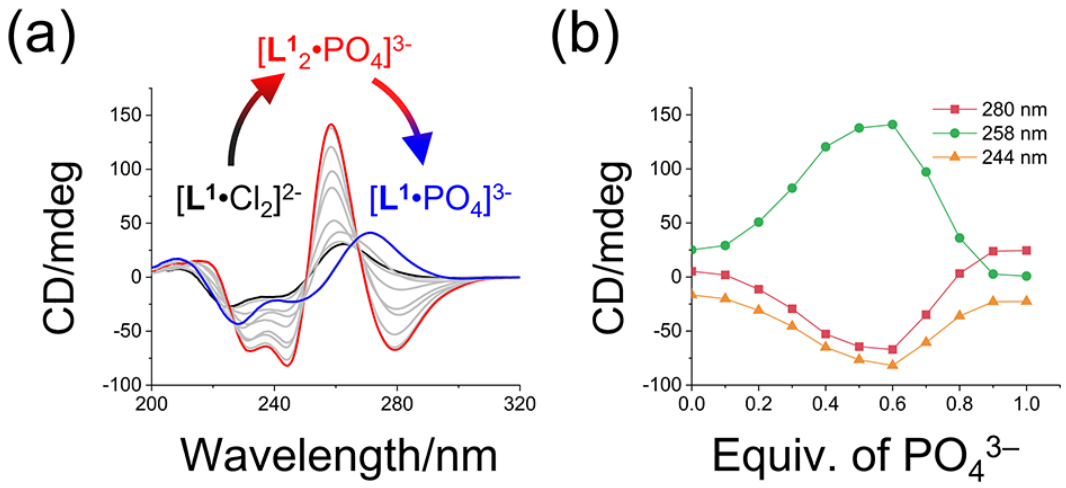

Figure S5. (a) CD spectra of $[\mathbf{L^1}\bullet Cl_2]^{2-}$ by adding 1 equivalent of phosphate anions gradually showing conversion in helical sense and (b) changes in CD spectra at wavelength of 244 nm, 258 nm and 280 nm. ($[\mathbf{L^1}]$ = 30 μM, CH_3CN)

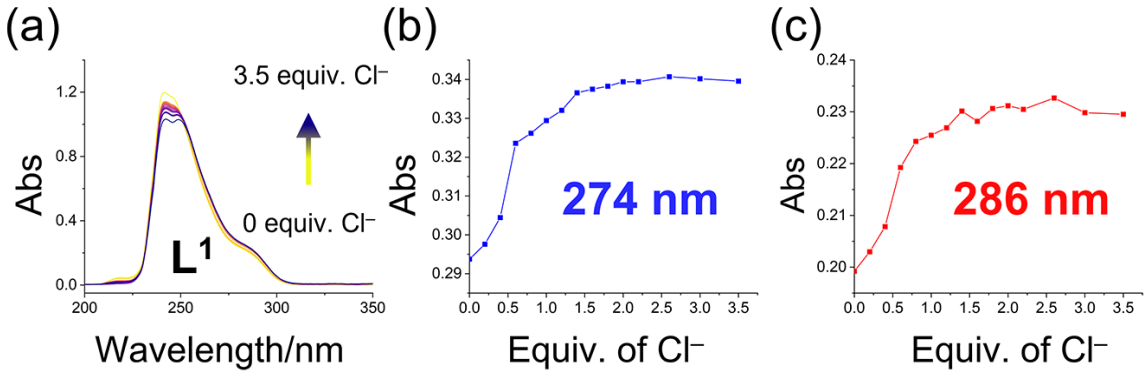

Figure S6. (a) UV-vis titration of $\mathbf{L^1}$ ($[\mathbf{L^1}]$ = 30 μM) with Cl^- in 5% v/v DMSO/CH_3CN and (b) changes in UV-vis spectra at wavelength of 274 nm and 286 nm.

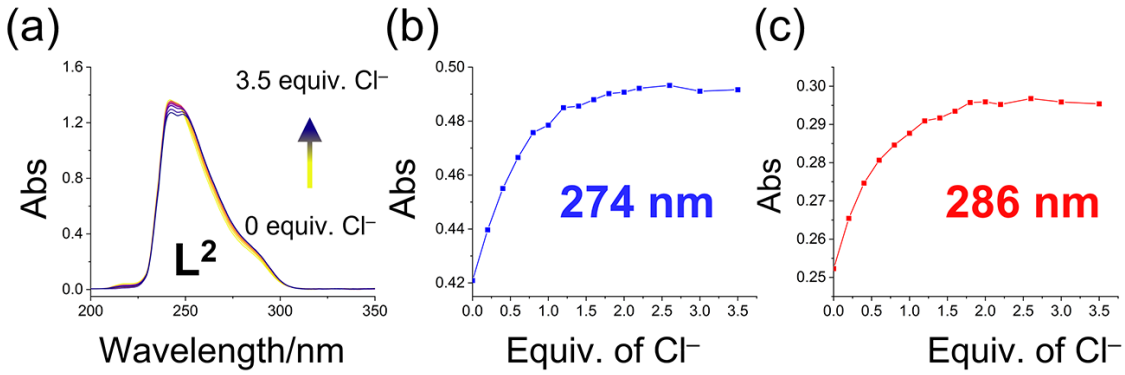

Figure S7. (a) UV-vis titration of $\mathbf{L^2}$ ($[\mathbf{L^2}]$ = 30 μM) with Cl^- in 5% v/v DMSO/CH_3CN and (b) changes in UV-vis spectra at wavelength of 274 nm and 286 nm.

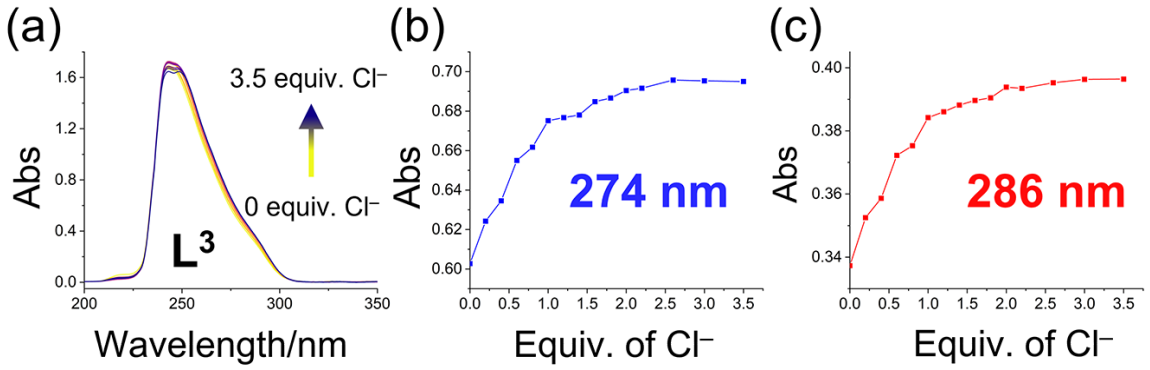

Figure S8. (a) UV-vis titration of $\mathbf{L^3}$ ([$\mathbf{L^3}$] = 30 μM) with Cl^- in 5% v/v DMSO/CH_3CN and (b) changes in UV-vis spectra at wavelength of 274 nm and 286 nm.

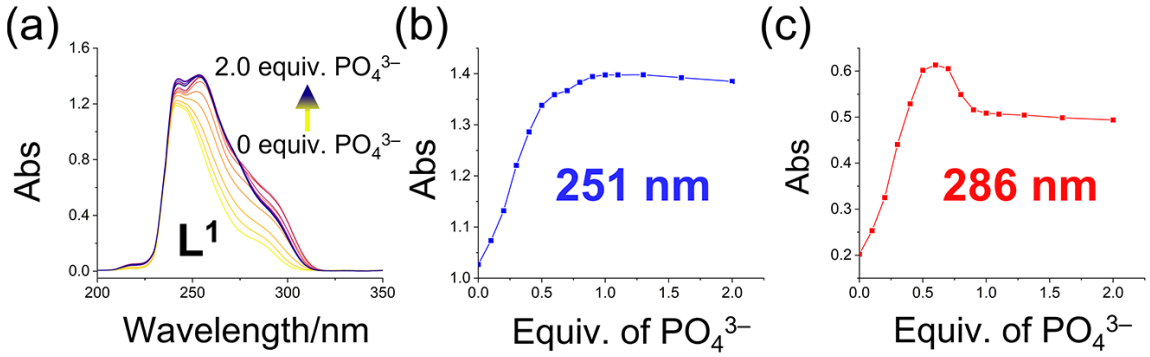

Figure S9. (a) UV-vis titration of $\mathbf{L^1}$ ([$\mathbf{L^1}$] = 30 μM) with PO_4^{3-} in 5% v/v DMSO/CH_3CN and (b) changes in UV-vis spectra at wavelength of 251 nm and 286 nm.

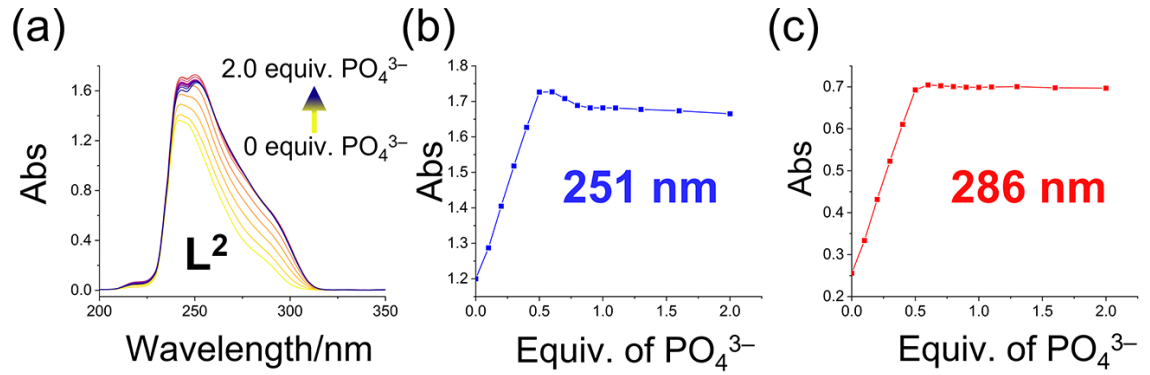

Figure S10. (a) UV-vis titration of $\mathbf{L^2}$ ([$\mathbf{L^2}$] = 30 μM) with PO_4^{3-} in 5% v/v DMSO/CH_3CN and (b) changes in UV-vis spectra at wavelength of 251 nm and 286 nm.

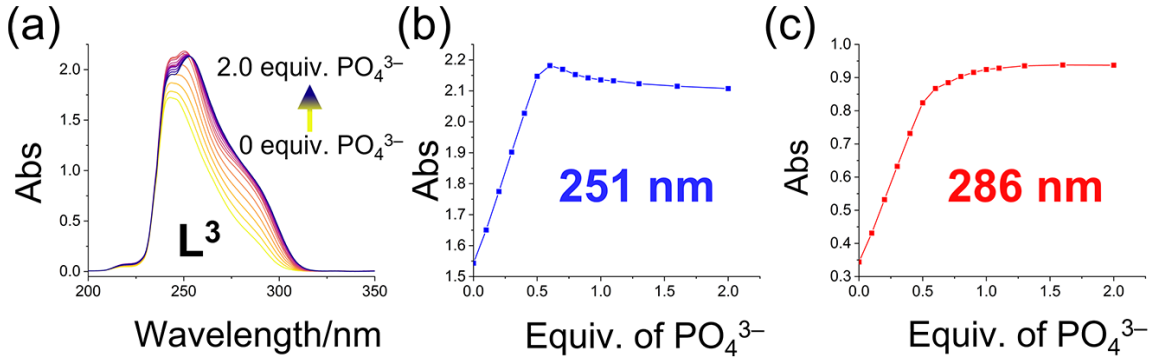

Figure S11. (a) UV-vis titration of $\mathbf{L^2}$ ([$\mathbf{L^2}$] = 30 μM) with PO_4^{3-} in 5% v/v DMSO/CH_3CN and (b) changes in UV-vis spectra at wavelength of 251 nm and 286 nm.

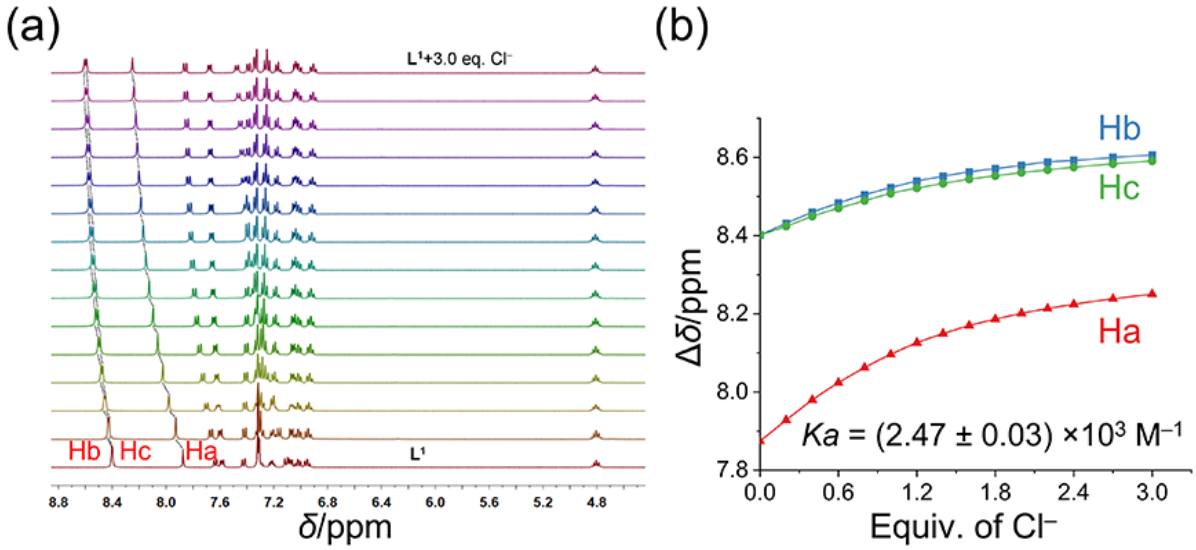

Figure S12. (a) ^{1}H NMR titration (400 MHz, DMSO-d_6, 298 K) of $\mathbf{L^1}$ ([$\mathbf{L^1}$] = 0.6 mM) in the presence of various equiv. of chloride anions and (b) the corresponding binding constants were obtained from non-linear curve-fitting to a 1:1 binding model via the http://app.supramolecular.org/bindfit/view/dbcb92af-4e2f-4125-8090-3f3debdeb6d5.

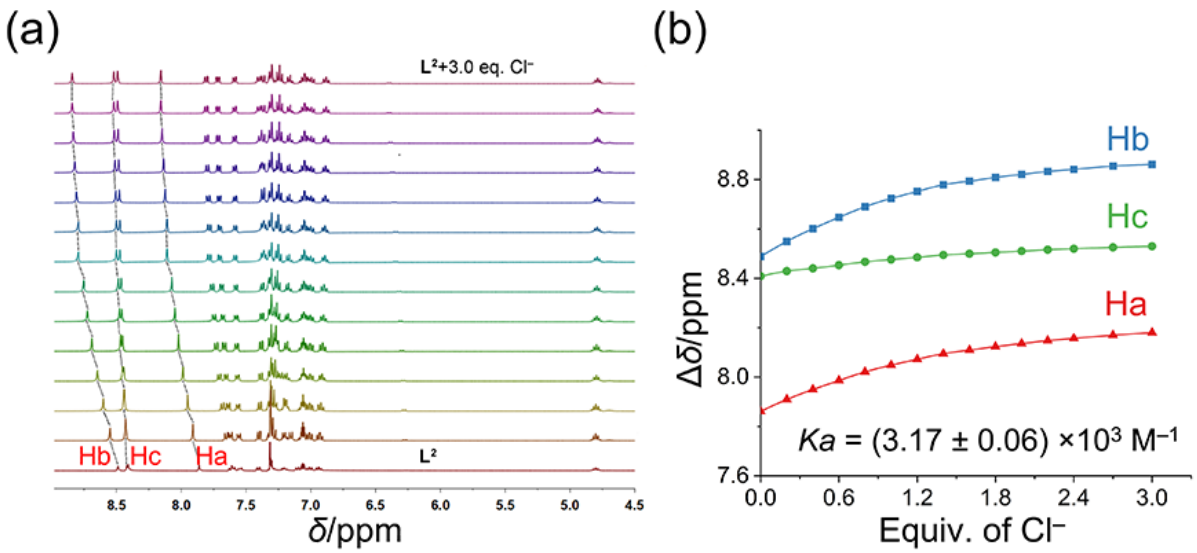

Figure S13. (a) ^{1}H NMR titration (400 MHz, DMSO-d_6, 298 K) of **L²** ([**L²**] = 0.6 mM) in the presence of various equiv. of chloride anions and (b) the corresponding binding constants were obtained from non-linear curve-fitting to a 1:1 binding model via the http://app.supramolecular.org/bindfit/view/83e937a4-7503-4b85-b5e5-82ced312fff2.

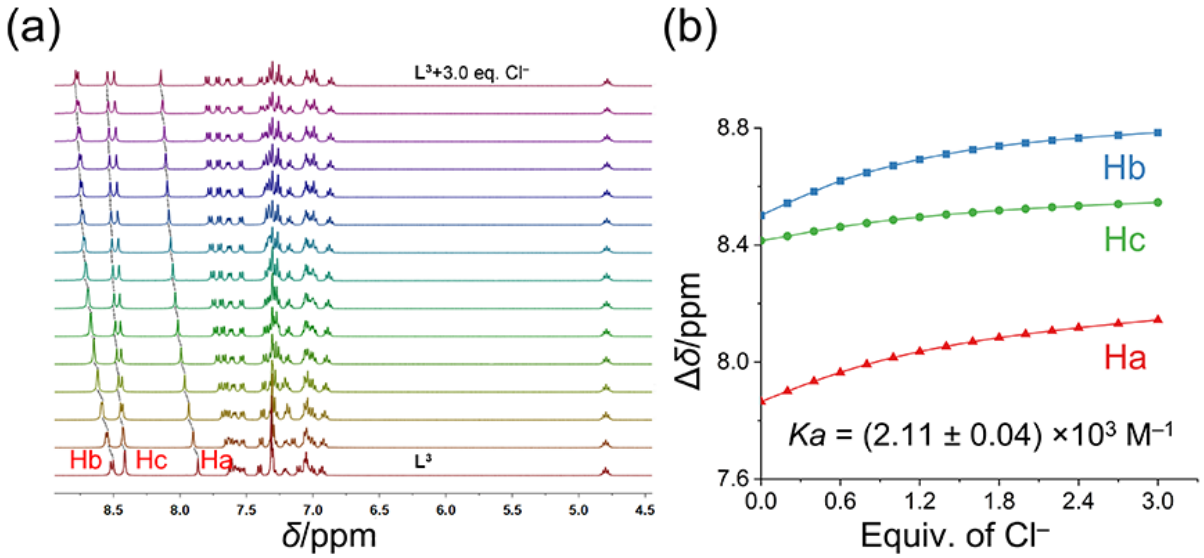

Figure S14. (a) ^{1}H NMR titration (400 MHz, DMSO-d_6, 298 K) of **L³** ([**L³**] = 0.6 mM) in the presence of various equiv. of chloride anions and (b) the corresponding binding constants were obtained from non-linear curve-fitting to a 1:1 binding model via the http://app.supramolecular.org/bindfit/view/9e915224-125e-4066-9fa8-03657d6d3e63.

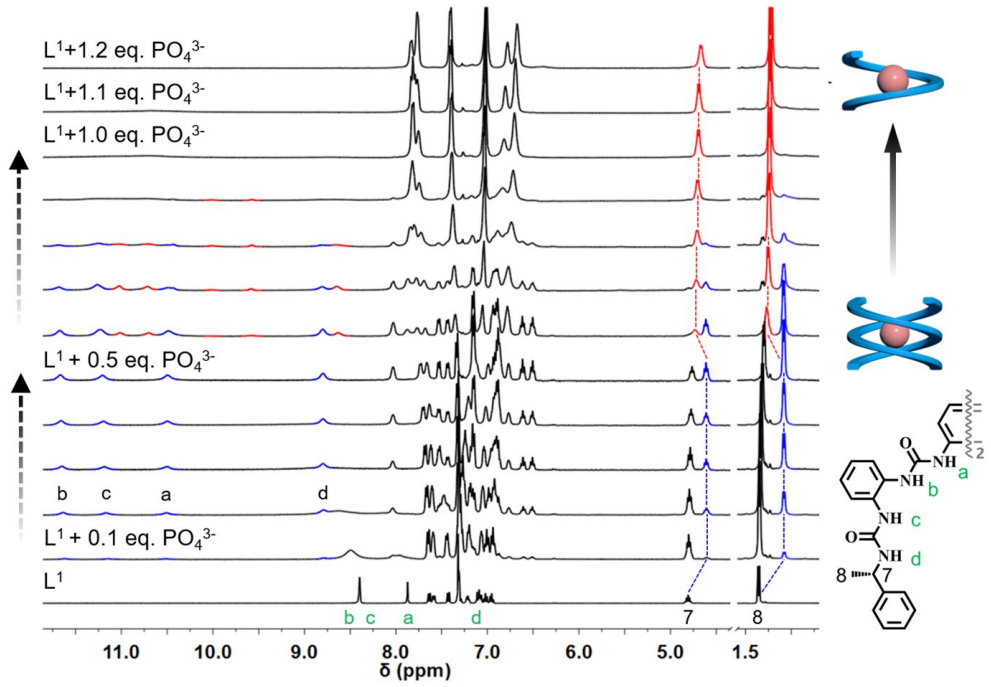

Figure S15. Partial ^{1}H NMR (400 MHz, DMSO-*d*$_6$, 298 K) spectra of **L^1** ([**L**] = 0.1 mM) in the presence of various equivalent of PO_4^{3-} (black numbers indicate the equivalent of PO_4^{3-} added; the signals of *MM* and *P* are shown in blue and red, respectively).

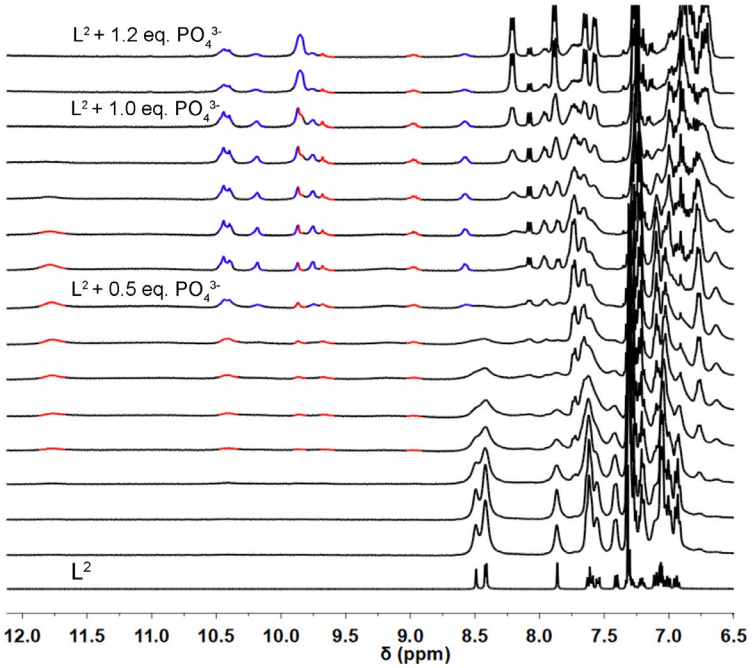

Figure S16. Partial ^{1}H NMR (400 MHz, DMSO-*d6*, 298 K) spectra of **L^2** ([**L**] = 0.1 mM) in the presence of various equivalent of PO_4^{3-} (black numbers indicate the equivalent of PO_4^{3-} added; the signals of $[\mathbf{L^2}_2{\bullet}PO_4]^{3-}$ and $[\mathbf{L^2}{\bullet}PO_4]^{3-}$ complexes are shown in blue and red, respectively).

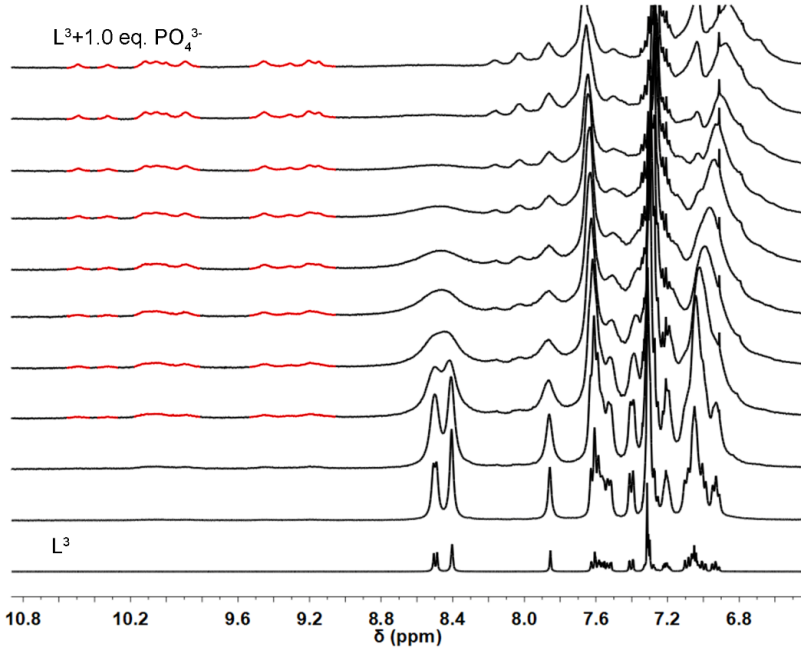

Figure S17. Partial ^{1}H NMR (400 MHz, DMSO-*d6*, 298 K) spectra of $\mathbf{L^3}$ ([**L**] = 0.1 mM) in the presence of various equivalent of PO_4^{3-} (black numbers indicate the equivalent of PO_4^{3-} added; the signals of $[\mathbf{L^3}\bullet PO_4]^{3-}$ complex are shown in red).

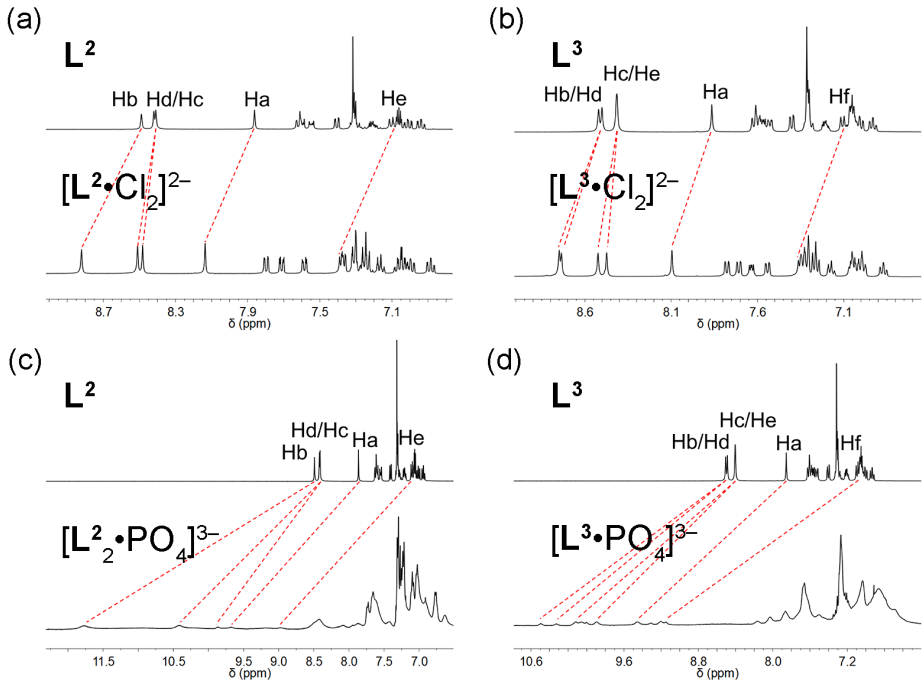

Figure S18. Stacked partial ^{1}H NMR spectra (400 MHz, 298 K, DMSO-*d*$_6$) for the oligourea ligands with their anion coordination complex of (a) $[\mathbf{L^2}\bullet Cl_2]^{2-}$, (b) $[\mathbf{L^3}\bullet Cl_2]^{2-}$, (c) $[\mathbf{L^2}_2\bullet PO_4]^{3-}$,

and (d) $[\mathbf{L^3}\bullet PO_4]^{3-}$, respectively. Tetrabutylammonium chloride and tetramethylammonium phosphate salts were used.

Table S9. Chemical shift of NH signals for complexes **1-3** in ^{1}H NMR.

NH / Complex	Ha	Hb	Hc	Hd	He	Hf
1	0.32	0.18	0.16	0.32		
2	0.28	0.33	0.1	0.07	0.28	
3	0.23	0.25	0.11	0.22	0.06	0.25

Table S10. Chemical shift of NH signals for complexes **4-6** in ^{1}H NMR.

NH / Complex	Ha	Hb	Hc	Hd	He	Hf
4	2.60	3.30	2.85	1.69		
5	1.82	3.29	2.02	1.44	1.87	
6	1.61	1.98	1.72	1.84	1.49	2.11

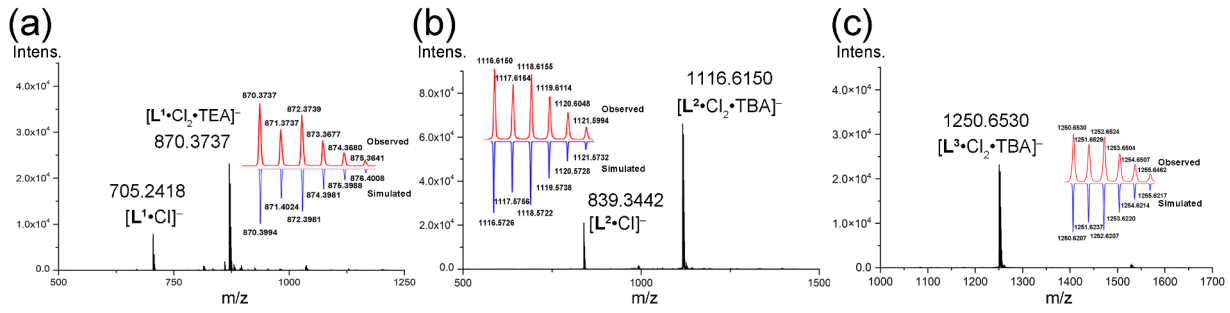

Figure S19. High-resolution ESI-MS spectrum of (a-c) complexes of oligourea ligands with two equivalents of chloride anion.

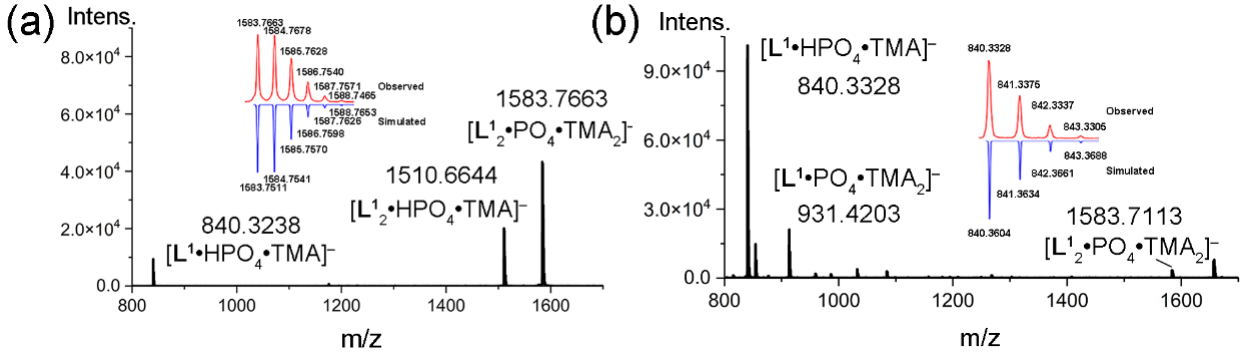

Figure S20. High-resolution ESI-MS spectrum of the formation of (a) double helix $[\mathbf{L^1}_2\bullet PO_4]^{3-}$ and (b) single helix $[\mathbf{L^1}\bullet PO_4]^{3-}$.

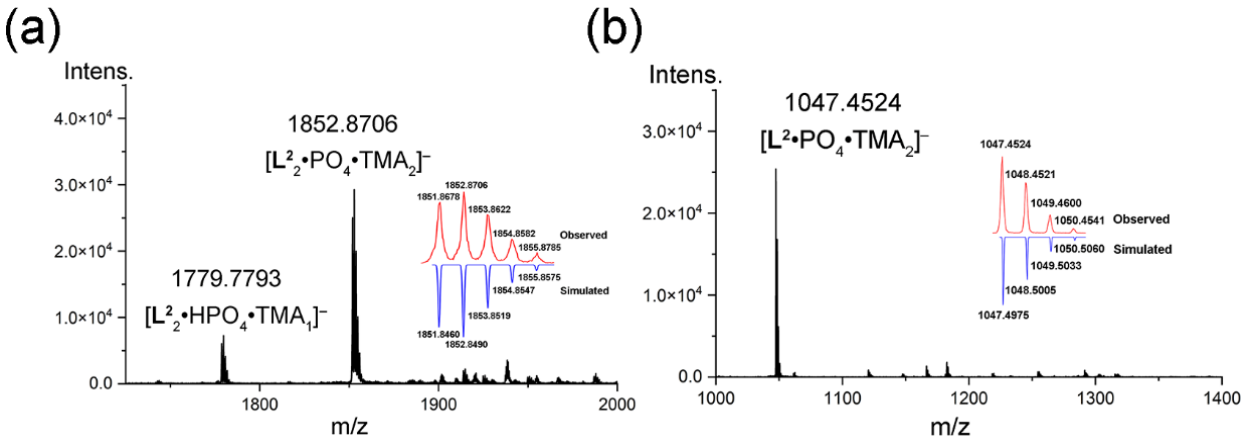

Figure S21. High-resolution ESI-MS spectrum of the formation of (a) $[\mathbf{L}^{\mathbf{2}}{}_2\bullet PO_4]^{3-}$ and (b) $[\mathbf{L}^{\mathbf{2}}\bullet PO_4]^{3-}$.

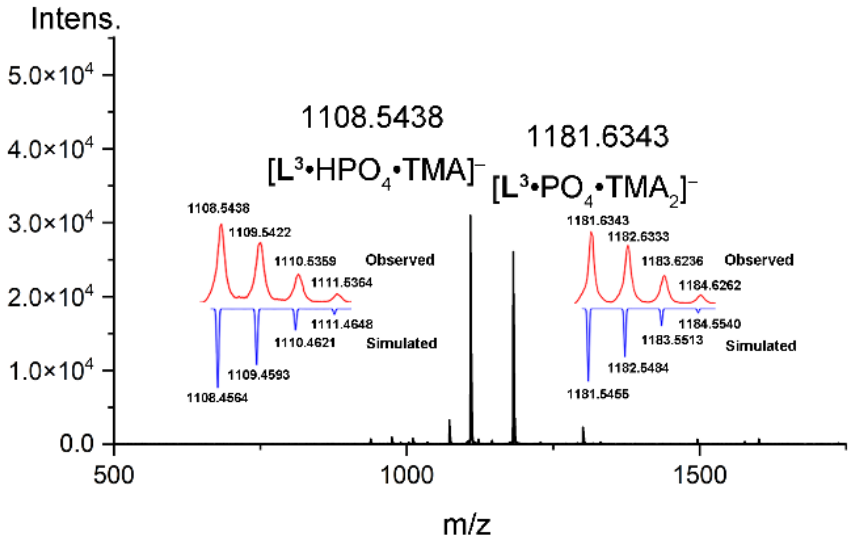

Figure S22. High-resolution ESI-MS spectrum of the formation of single helix $[\mathbf{L}^{\mathbf{3}}\bullet PO_4]^{3-}$.

S7. Computational Analysis for the Helicity Bias

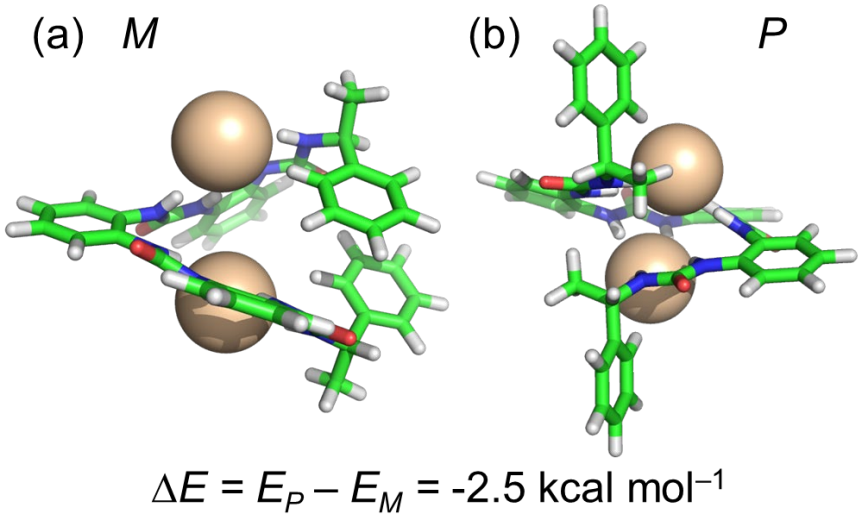

Figure S23. Computationally optimized geometry (DFT, B3LYP, 6-31G*) for the single helix of $[\mathbf{L^1}\bullet Cl_2]^{2-}$ with (a) left-handed conformation *M* and (b) right-handed conformation *P*. The optimized structure indicates that the right-handed helix is more stable than the left-handed helix.

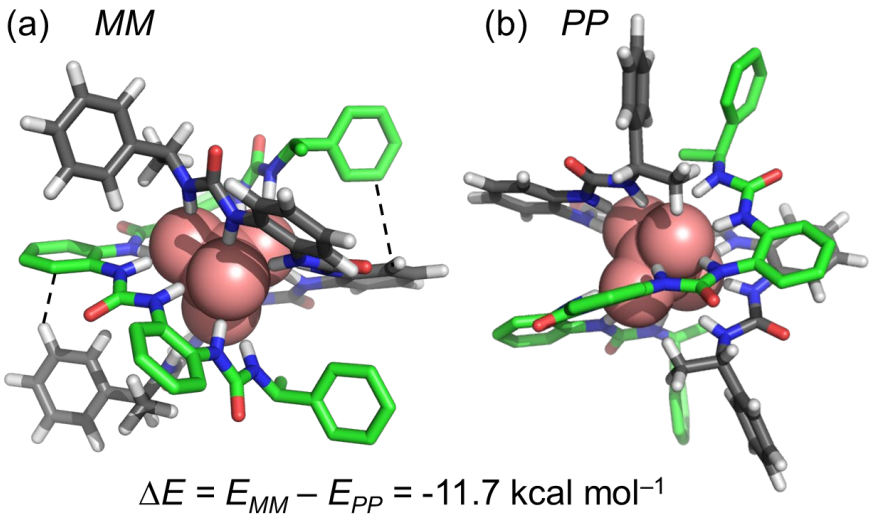

Figure S24. Computationally optimized geometry (DFT, B3LYP, 6-31G*) for the double helices of $[\mathbf{L^1}_2\bullet PO_4]^{3-}$ with (a) left-handed conformation *MM* and (b) right-handed conformation *PP*. The results suggests that the left-handed double helices is more energetically favorable than the right-handed double helices. And the extra contact of C-H•••π interaction between the strands of *MM* conformations could be driving force for the induced helicity bias.

S8. ^{1}H and ^{13}C NMR Spectra

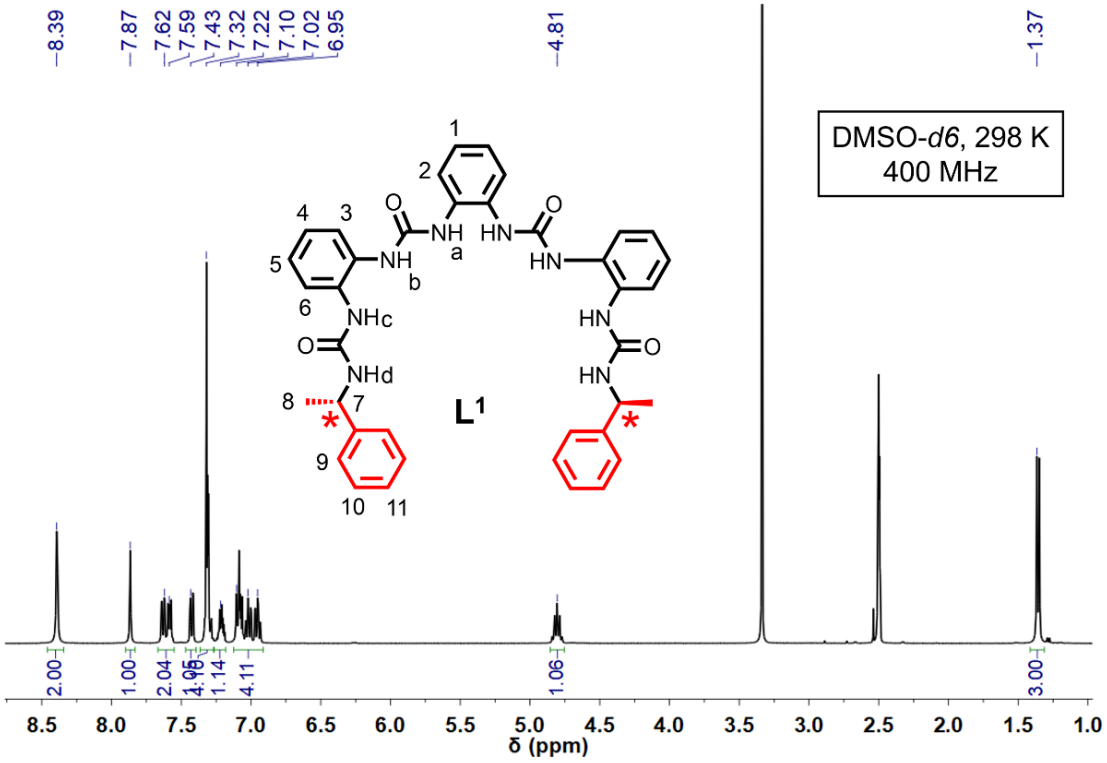

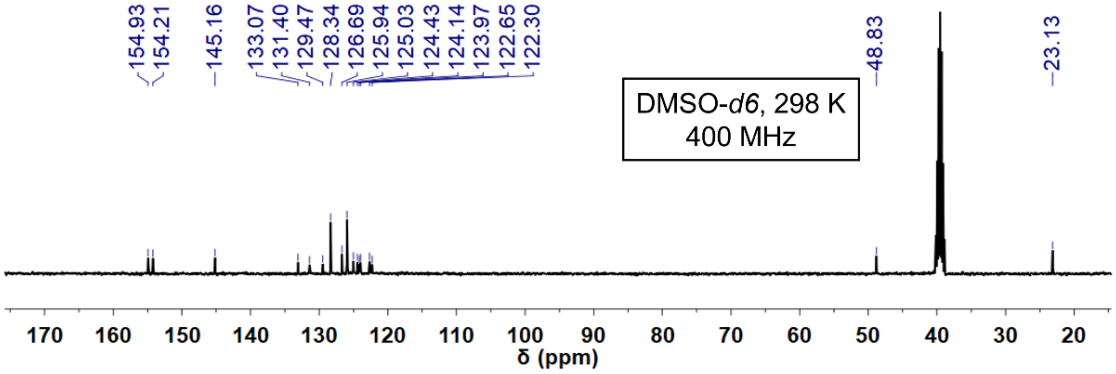

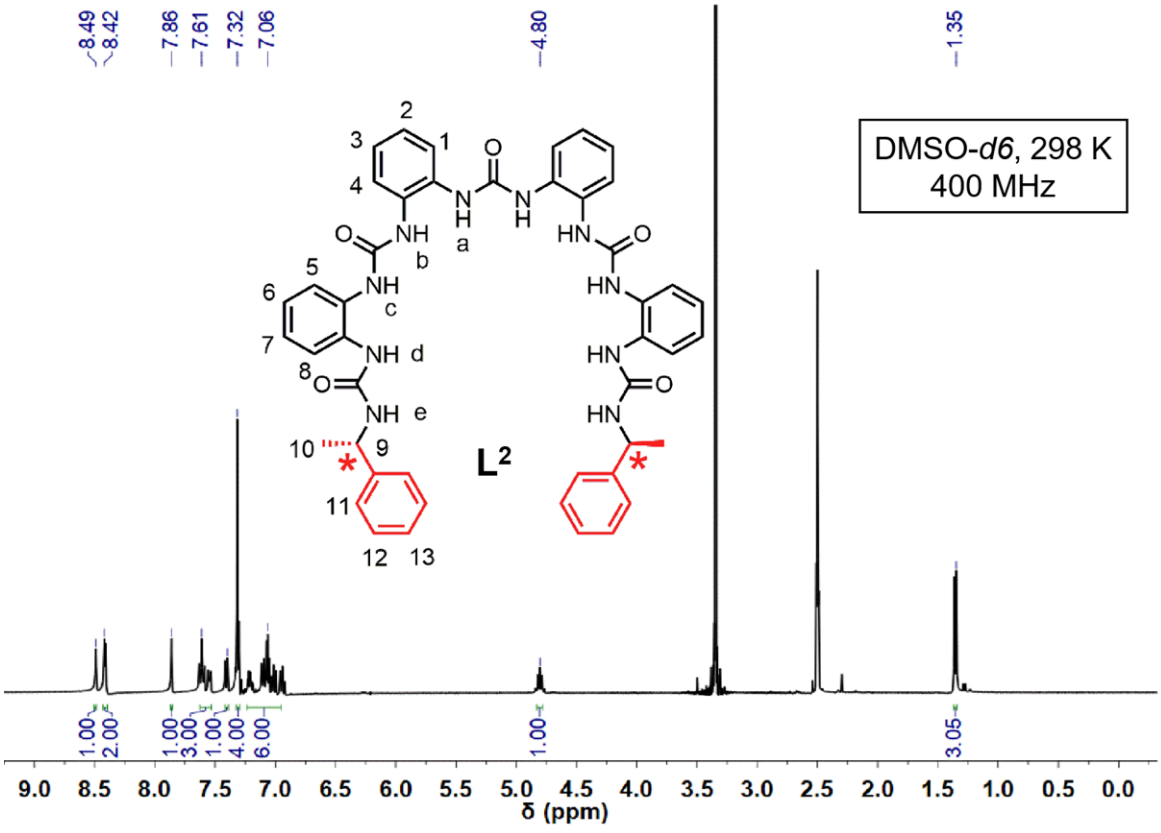
8.49
8.42
7.86
7.61
7.32
7.06
4.80
1.35
DMSO-d6, 298 K
400 MHz
L2
1.00
2.00
1.00
3.00
1.00
4.00
6.00
1.00
3.05
9.0 8.5 8.0 7.5 7.0 6.5 6.0 5.5 5.0 4.5 4.0 3.5 3.0 2.5 2.0 1.5 1.0 0.5 0.0
δ (ppm)

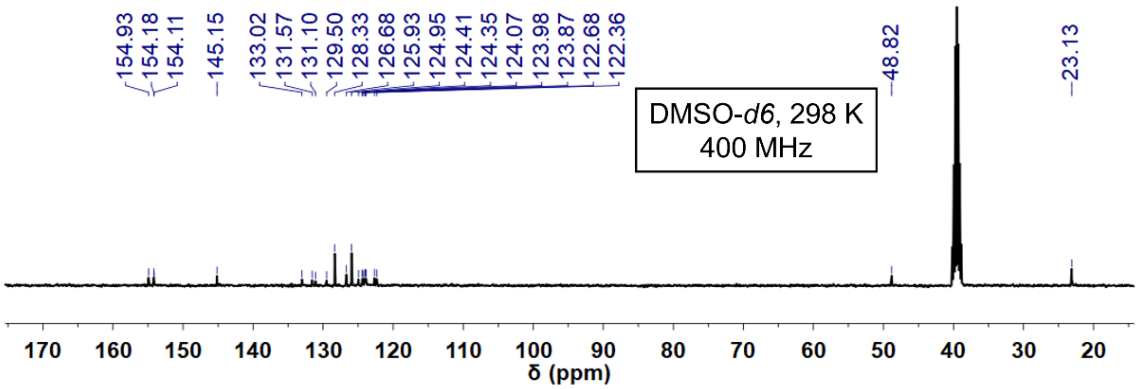
154.93
154.18
154.11
145.15
133.02
131.57
131.10
129.50
128.33
126.68
125.93
124.95
124.41
124.35
124.07
123.98
123.87
122.68
122.36
48.82
23.13
DMSO-d6, 298 K
400 MHz
170 160 150 140 130 120 110 100 90 80 70 60 50 40 30 20
δ (ppm)

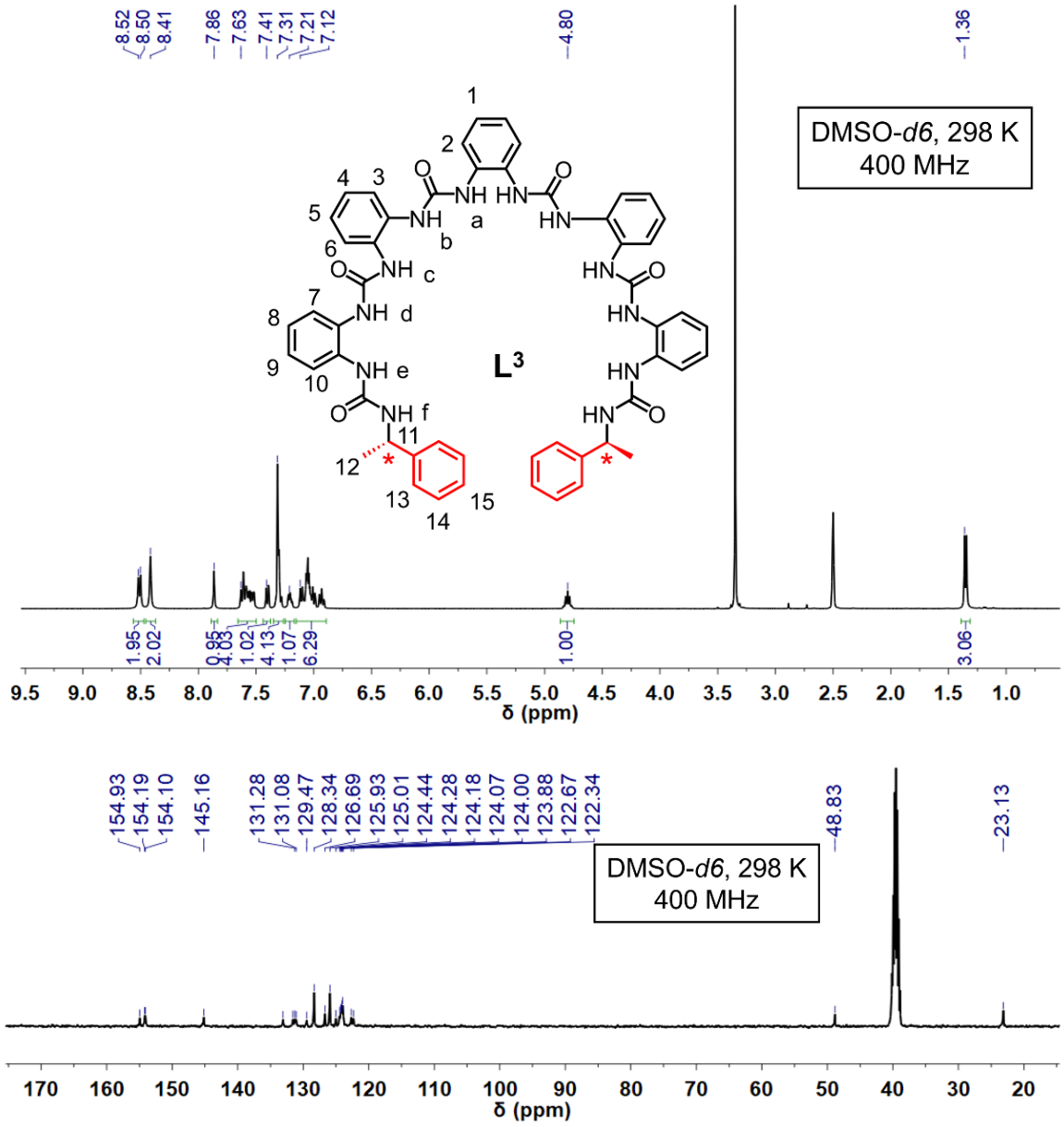
8.52
8.50
8.41
7.86
7.63
7.41
7.31
7.21
7.12
4.80
1.36
DMSO-d6, 298 K
400 MHz
L3
1.95
2.02
0.85
4.03
1.02
4.13
1.07
6.29
1.00
3.06
δ (ppm)

154.93
154.19
154.10
145.16
131.28
131.08
129.47
128.34
126.69
125.93
125.01
124.44
124.28
124.18
124.07
124.00
123.88
122.67
122.34
48.83
23.13
DMSO-d6, 298 K
400 MHz
δ (ppm)